Available online at www.sciencedirect.com
ScienceDirect
Journal of Power Sources 174 (2007) 16–29
JOURNAL OF POWER SOURCES
www.elsevier.com/locate/jpowsour

VRLA Ultrabattery for high-rate partial-state-of-charge operation

L.T. Lam [a,*], R. Louey [a], N.P. Haigh [a], O.V. Lim [a], D.G. Vella [a], C.G. Phyland [a], L.H. Vu [a], J. Furukawa [b], T. Takada [b], D. Monma [b], T. Kano [b]

[a] *CSIRO Energy Technology, Box 312, Clayton South, Victoria 3169, Australia*
[b] *The Furukawa Battery Co. Ltd., Japan*

Received 15 March 2007; received in revised form 15 May 2007; accepted 16 May 2007
Available online 21 May 2007

Abstract

The objective of this study is to produce and test the hybrid valve-regulated Ultrabattery designed specifically for hybrid-electric vehicle duty, i.e., high-rate partial-state-of-charge operation. The Ultrabattery developed by CSIRO Energy Technology is a hybrid energy-storage device, which combines an asymmetric supercapacitor, and a lead-acid battery in one unit cells, taking the best from both technologies without the need for extra, expensive electronic controls. The capacitor will enhance the power and lifespan of the lead-acid battery as it acts as a buffer during high-rate discharging and charging. Consequently, this hybrid technology is able to provide and absorb charge rapidly during vehicle acceleration and braking. The work programme of this study is divided into two main parts, namely, field trial of prototype Ultrabatteries in a Honda Insight HEV and laboratory tests of prototype batteries. In this paper, the performance of prototype Ultrabatteries under different laboratory tests is reported.

The evaluation of Ultrabatteries in terms of initial performance and cycling performance has been conducted at both CSIRO and Furukawa laboratories. The initial performance of prototype Ultrabatteries, such as capacity, power, cold cranking and self-discharge has been evaluated based upon the US FreedomCAR Battery Test Manual (DOE/ID-11069, October 2003). Results show that the Ultrabatteries meet, or exceed, respective targets of power, available energy, cold cranking and self-discharge set for both minimum and maximum power-assist HEVs. The cycling performance of prototype Ultrabatteries has been evaluated using: (i) simplified discharge and charge profile to simulate the driving conditions of micro-HEV; (ii) 42-V profile to simulate the driving conditions of mild-HEV and (iii) EUCAR and RHOLAB profiles to simulate the driving conditions of medium-HEV. For comparison purposes, nickel–metal-hydride (Ni–MH) cells, which are presently used in the Honda Insight HEV, have also been subjected to some of the above profiles (i.e., simplified discharge and charge profile and EUCAR profile). Although the Ultrabattery and a Ni–MH cell under EUCAR test profile are still on cycling, the outcomes to date show that the performance of these batteries and cells has been at least four times longer than that of the state-of-the art lead-acid cells or batteries. Excitingly, the performance of Ultrabatteries is proven to be comparable with that of the Ni–MH cells.

Keywords: Asymmetric supercapacitor; Lead-acid battery; Ultrabattery; High-rate partial-state-of-charge operation; Hybrid-electric vehicles; Available energy

1. Hybrid-electric vehicles and energy-storage systems

Transport is one of the largest sources of human-induced greenhouse gas emissions and fossil-fuels consumption. Thus, the ideal future transport should be directed towards the use of zero-emission vehicles on a life cycle basis. This encompasses electric vehicles and/or fuel-cell vehicles, which use alternative fuel, such as hydrogen produced without greenhouse gas emissions. Since these vehicles are still under development and improvement, lower emission and lower fuel consumption, hybrid-electric vehicles (HEVs) have been developed and commercialized for use during this transition phase.

There are several types of HEVs, namely, micro-, mild-, medium- and full-hybrid (Table 1). Each type of vehicle requires the batteries to operate in a slightly different way. For micro-hybrid vehicles, the battery is required to receive energy from regenerative braking and provide energy to start the vehicle. For mild- and medium-hybrid vehicles, in addition to regenerative braking and engine start, the battery is required to supply energy for acceleration (e.g., motor assist). For full-hybrid vehicles, the battery is further required to supply energy for short distances of pure electric driving, especially in the urban areas. The system voltage of the HEVs increases from 12 V in the micro-hybrid to over 200 V in the full-hybrid, while the battery capacity

* Corresponding author. Tel.: +61 3 9545 8401; fax: +61 3 9545 8403.
E-mail address: lan.lam@det.csiro.au (L.T. Lam).

0378-7753/$ – see front matter © 2007 Elsevier B.V. All rights reserved.
doi:10.1016/j.jpowsour.2007.05.047

Table 1
Types of hybrid-electric vehicles

	Micro	Mild	Medium	Full
Regenerative braking	★	★	★★	★★★
Engine start	★	★	★	★
Motor assist		★	★★	★★★
EV drive				★
Battery voltage (V)	12	36	144	>200
Battery capacity (Ah)	50–60	15–20	6–8	6

Note: blank = no requirement; one star = mild requirement; two stars = medium requirement; three stars = strong requirement.

decreases from 50 to 60 Ah in the micro-hybrid to only 6 Ah in the full-hybrid. All types of hybrid-electric vehicles demand the battery to be discharged and charged at high rates under partial-state-of-charge condition, so called 'HRPSoC duty'. High-rate discharge is necessary for engine cranking and acceleration, while high-rate charge is associated with regenerative braking.

At present, candidate energy-storage systems for HEV applications include valve-regulated lead-acid (VRLA), nickel–metal-hydride (Ni–MH), rechargeable lithium batteries and supercapacitor. It needs to state here that flooded-electrolyte lead-acid battery is also considered to be used in micro- and mild-HEVs. It is obvious that the VRLA battery has great advantages in terms of low initial (capital) cost, well-established manufacturing base, distribution networks and high recycling efficiency compared to the other competitive technologies at their current stage of development. Nevertheless, the running cost of the VRLA battery is expensive because of the short service life. The VRLA battery under HEV applications must be operated within a certain state-of-charge (SoC) window, i.e., 30–70% SoC (Fig. 1). This is because the battery cannot deliver the required cranking current when the SoC is below 30%. On the other hand, the battery cannot accept charge efficiently either from regenerative braking or from engine charging when the SoC is above 70%. Under such applications, the VRLA battery fails prematurely due to the sulfation of the plates, particularly the negative plates [1–5]. The negative plates suffer from a progressive build-up of 'hard' lead sulfate on the surface, i.e., lead sulfate, which is difficult to recharge. The accumulation of lead sulfate markedly reduces the effective surface-area to such extent that the plate can no longer deliver and accept the power required by engine cranking, acceleration and regenerative braking.

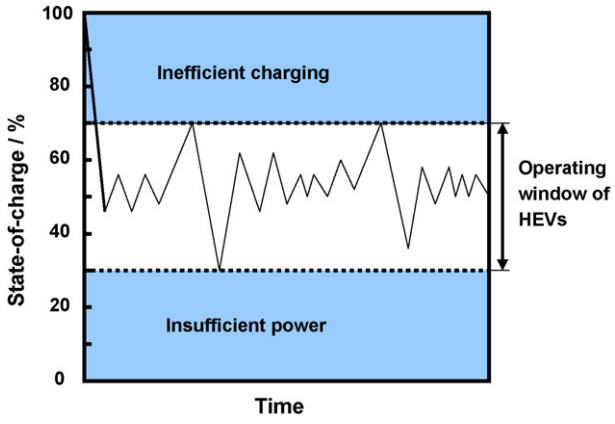

Fig. 1. State-of-charge window for lead-acid battery operated in HEVs.

2. Mechanism of lead sulfate accumulation in negative plates under HRPSoC duty

The mechanism of lead sulfate accumulation on the surfaces of negative plates under HRPSoC duty has been documented in the previous paper [6]. The key factors responsible for such accumulation of lead sulfate are the high-rate discharge and charge. During high-rate discharging, the sponge Pb reacts with HSO_4^- to form $PbSO_4$ and this reaction proceeds so rapidly that the diffusion rate of HSO_4^- from the bulk of the solution cannot catch up with its consumption rate in the interior of negative plate. Moreover, high-rate discharge generates a very high supersaturation of Pb^{2+} in the vicinity of each parent lead crystal. The lead sulfate will therefore precipitate rapidly on any available surface, irrespective of whether this be sponge lead or already-deposited lead sulfate, i.e., nucleation rate > growth rate. Thus, a compact layer of tiny lead sulfate crystals will develop on the surface of the plate (Fig. 2). This will reduce the effective surface-area for electron transfer and will also hinder the diffusion of HSO_4^- into the interior of the plate (note, the dense lead sulfate layer acts as a semi membrane to the movement of HSO_4^-). During subsequent high-rate charging, the negative-plate potential increases to such extent that, given the lower level of sulfate in the plate interior, the charging current during passage from the grid member to the plate surface reduces some hydrogen ions to hydrogen gas before reaching the lead sulfate layer (Fig. 3). Thus, complete conversion of lead sulfate at the plate surface cannot be achieved. With such repetitive action of high-rate discharge and charge, the lead sulphate will accumulate on the surfaces of negative plate and eventually, the battery will be unable to provide sufficient power for engine cranking.

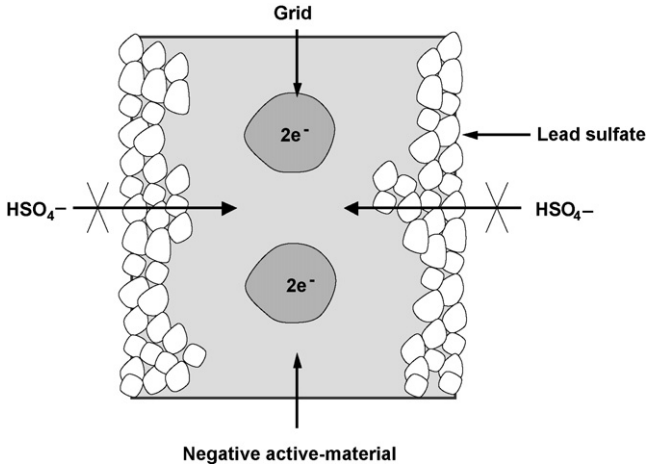

Fig. 2. Schematic representation of the distribution of lead sulfate in a negative plate subjected to high-rate discharge.

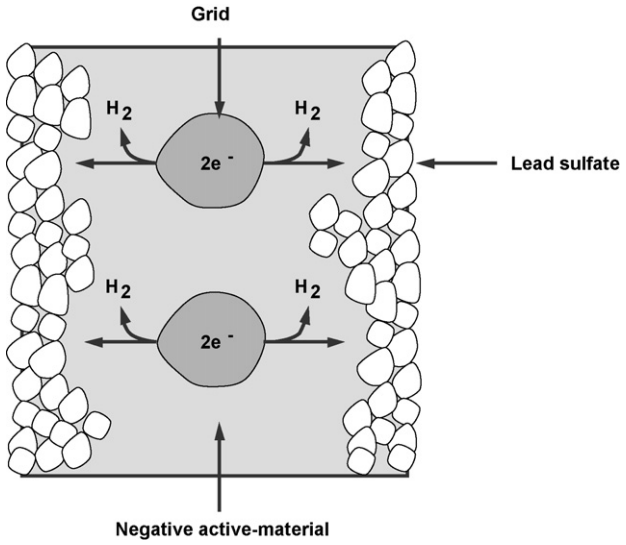

Fig. 3. Schematic representation of the charging process of a negative plate after high-rate discharge.

3. Approach to improve cycleability of VRLA batteries under HRPSoC duty

From the above discussion, it is clear that in order to improve the cycleability of VRLA batteries under HRPSoC duty, the uneven distribution of lead sulfate across the cross-section of negative plate during discharge and the early evolution of hydrogen during charge should be minimized. With these considerations, several approaches have been taken.

(i) Localization of charging current on plate surface

It is obvious that the lead sulfate layer can be converted more effectively when the charging current can be concentrated on the surface of the negative plate. The localization of charging current, in fact, can be achieved by the superimposition of pulsed current of high frequency to the battery during charging—the higher the frequency, the greater is the amount of current concentrated on the plate surface. This phenomenon is known as the 'skin effect' as only the outer 'skin' of the plate is effectively carrying the current. The use of the pulsed technique to minimize the build-up of lead sulfate layer has been studied in a project funded by the Advanced Lead-Acid Battery Consortium [1–3,5,6].

(ii) Addition of carbon

The use of carbon can minimize the uneven distribution of lead sulfate within the cross-section of negative plate. The high surface-area of carbon reduces the discharge and charge current densities. The porosity and the acid-affinity characteristics of carbon provide many acid reservoirs within the interior of the plate and these reservoirs give rise to active sites for the development of lead sulfate during discharge. Also, the carbon provides the conductive network to assist the subsequent charging process [7–10,4].

(iii) Plate-processing conditions, electrolyte concentration and addition of trace elements

The uneven distribution of lead sulfate in the negative plate of a lead-acid battery during cycling is dependent upon the surface-area, rates of discharge and charge, as well as the diffusion of HSO_4^- between the interior of the plate and the bulk of the electrolyte. Obviously, the latter is affected strongly by the plate-material density, thickness and electrolyte concentration. Thus, optimization of these parameters, together with the addition of trace elements (for suppressing the early evolution of hydrogen during charging) are expected to improve the cycle-life of the VRLA battery under HRPSoC duty. Such study has been conducted through a project also funded by the Advanced Lead-Acid Battery Consortium [11].

(iv) Protection of lead-acid battery from high-rate discharge and charge

The key factors responsible for the uneven distribution of lead sulfate in the negative plate and the early evolution of hydrogen are both the high-rate discharge and charge. To extend the life of a lead-acid battery, the negative plates should therefore be protected from high-rate discharge and charge. The conventional way to improve the life of the lead-acid battery is to connect the battery pack in parallel with a supercapacitor (Fig. 4). It is well

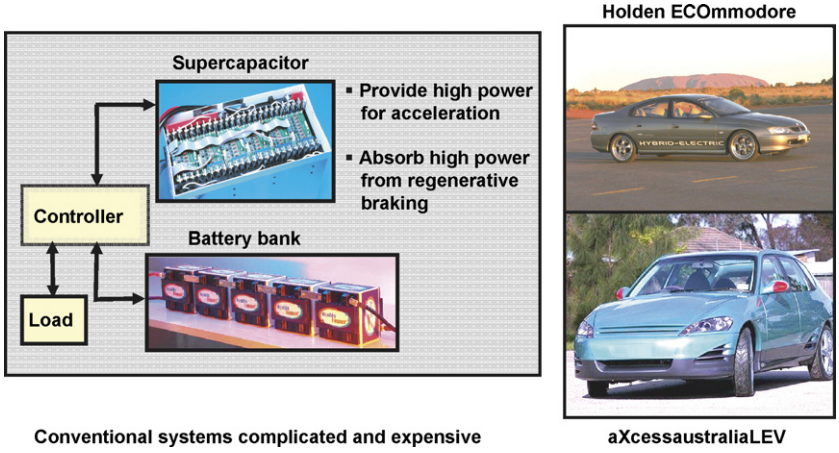

Fig. 4. Combined supercapacitor and lead-acid battery.

known that a supercapacitor can provide and receive high power, but low energy and therefore, for HEV applications, the best use of this technology is to absorb high power from regenerative braking and to provide high power for acceleration. The energy and power flow between the capacitor and battery pack are controlled by an electronic controller. In principle, during vehicle braking and acceleration, the controller will first regulate the power to and from the supercapacitor, then the battery pack. During engine charging and cruise driving, the controller will regulate the power and energy mainly to and from the battery pack. This system has been developed by CSIRO and has been used successfully in the Holden ECOmmodore and aXcessaustralia demonstration cars in the year 2000. Nevertheless, the drawbacks of this system are that it is complicated (e.g., requires a sophisticated algorithm) and is expensive.

4. Ultrabattery—A solution for valve-regulated lead-acid battery as electric power source for HEV applications

Accordingly, CSIRO Energy Technology has developed an advanced Ultrabattery to replace the complex and high cost supercapacitor/lead-acid battery system [12–14]. The schematic configuration of the Ultrabattery is shown in Fig. 5. A lead-acid cell comprises one lead-dioxide positive plate and one sponge lead negative plate. On the other hand, an asymmetric supercapacitor composes of one lead-dioxide positive plate and one carbon-based negative plate (i.e., capacitor electrode). Since the positive plates in the lead-acid cell and the asymmetric supercapacitor have a common composition, these two devices can be integrated into one unit cell by internally connecting the capacitor electrode and the lead-acid negative plate in parallel. Both electrodes now share the same lead-acid positive plate. With this design, during discharge and charge, the total current of the combined negative plate is composed of two components: one is the capacitor current; the other is the lead-acid negative plate current. Accordingly, the capacitor electrode can now act as a

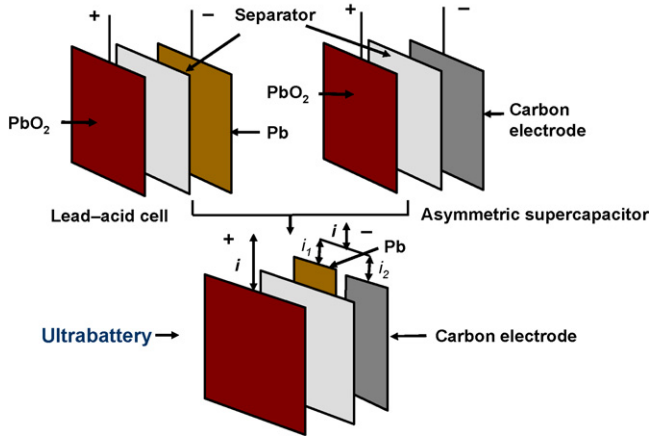

Fig. 5. Schematic diagram showing the configuration of Ultrabattery.

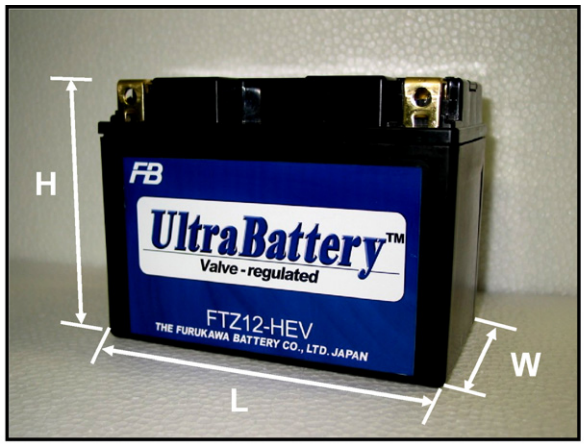

Dimensions of battery and grids

	Height (mm)	Width (mm)	Length/thickness (mm)
Battery	110	87	150
Positive grid	76	76	1.60
Negative grid	76	76	1.45

Fig. 6. Appearance and dimensions of prototype Ultrabattery.

buffer to share the discharge and charge currents with the lead-acid negative plate and thus prevent it from being discharged and charged at the full rates required by the HEV duty. The Ultrabattery is, in fact, a hybrid energy-storage device, which combines an asymmetric supercapacitor and a lead-acid battery in a unit cell, without extra, expensive, electronic control. The initial CSIRO laboratory results show that the discharge and charge power of the Ultrabattery is higher and its cycle-life is significantly longer than that of the conventional lead-acid counterpart. Furthermore, the Ultrabattery is able to be produced as either flooded-electrolyte or valve-regulated designs in the existing lead-acid factory and also able to reconfigure for a variety of applications, such as conventional automobile, power tool, forklift, high-power uninterruptible power supply and remote-area power supply [14].

Accordingly, CSIRO Energy Technology and The Furukawa Battery Co. Ltd. have cooperated in the production of prototype Ultrabatteries. Fourty-five, 12-V prototype Ultrabatteries have been produced at the Furukawa plant. The appearance and dimensions of the Ultrabattery and grids are shown in Fig. 6. Twelve batteries have been sent to Provector Limited, UK, for field trial in a Honda Insight HEV and the remaining batteries are for the laboratory tests at CSIRO and Furukawa. In this paper, the performance of prototype Ultrabatteries under different laboratory tests is reported.

5. Initial performance of prototype ultrabatteries

The initial performance of Ultrabatteries was evaluated in terms of capacity, power, cold cranking and self-discharge. There tests were based upon the US FreedomCAR Battery Test Manual [15].

Table 2
Cut-off voltages for various constant-current discharges

Discharge current (A)	Cut-off voltage (V)
0.1*C*	10.5
0.2*C*	10.5
0.33*C*	9.9
1*C*	9.6
5*C*	9
10*C*	9
15*C*	9

Note: *C* = nominal 1-h capacity of the battery.

5.1. Capacity

The battery was discharged at various constant currents to the corresponding cut-off voltages as given in Table 2. The discharge current and discharge time were plotted on logarithmic scales as shown in Fig. 7. The relationship between the discharge current and discharge time can be expressed by the following equation.

$$y = 14.491x^{-1.2869} \quad (1)$$

where y is time in hour and x is current in ampere. The 1- and 2-h capacities of the battery calculated from the above equation are 6.67 and 7.78 Ah, respectively. These two capacities will be used for the later cycling tests.

5.2. Power

The procedure to determine the maximum discharge and charge power of the battery at different depth-of-discharge (DoD) is shown in Fig. 8. This involved:

(i) after full charge, determined 1-h capacity, followed by a recharge;
(ii) allowed the battery to stand at open-circuit condition for 1 h;
(iii) removed 10% of 1-h capacity of the battery at 1-h rate (e.g., discharge to 10% DoD), followed by 1-h rest;
(iv) after rest, discharged and charged the battery with a constant current procedure for power determination;

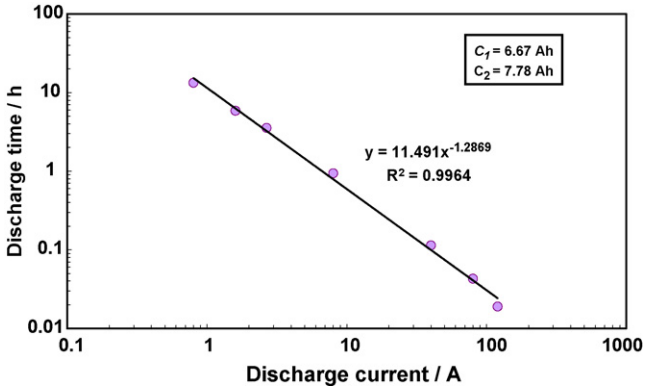

Fig. 7. Relationship between discharge current and time.

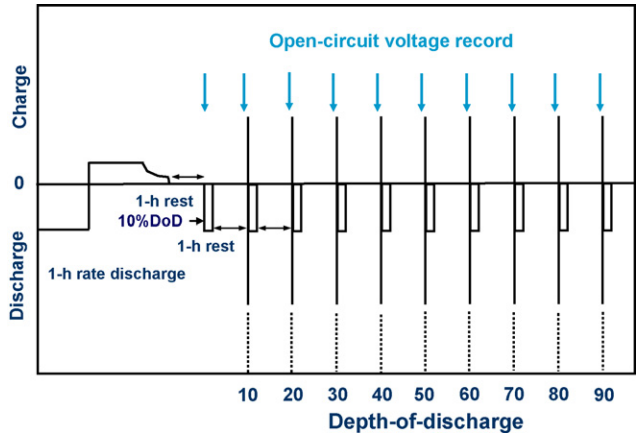

Fig. 8. Procedure to determine the discharge and charge power at different depth-of-discharge.

(v) repeated steps (iii) and (iv) until the DoD of the battery reached 90%;
(vi) discharged the battery to 100% DoD.

During test, the open-circuit voltage of the battery was recorded at the end of each 1-h rest period to determine the change in open-circuit voltage with depth-of-discharge.

The discharge– and charge–current profile used to determine the maximum discharge and charge power of the battery at a given DoD is shown in Fig. 9. After 1-h rest, the battery was discharged with a constant current of −8 C for 10 s, followed by 40-s rest. The battery was then recharged with a constant current of 6 C for 10 s. The current and the corresponding voltage were recorded before, and at the end of each pulse. The discharge resistance and the maximum power were calculated using the following equations with the minimum voltage (V_{min}) of 9 V.

$$R_{discharge} = \frac{\Delta V_{discharge}}{\Delta I_{discharge}} \quad (2)$$

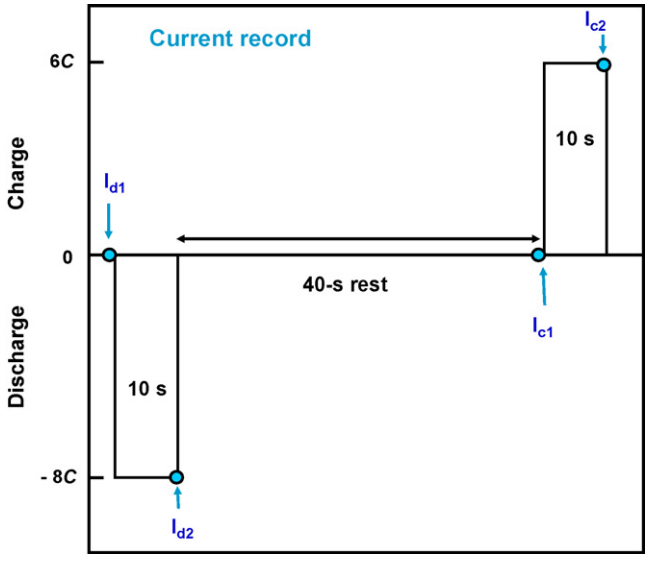

Fig. 9. Discharge– and charge–current profile used to determine the battery power.

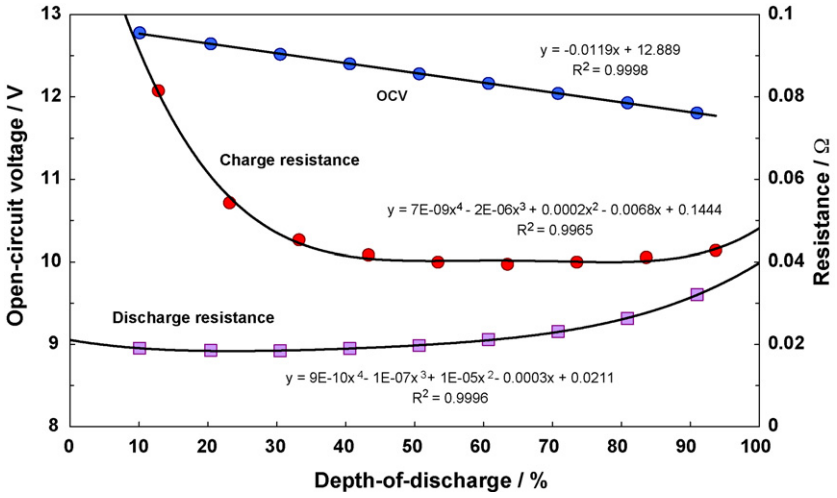

Fig. 10. Changes in open-circuit voltage, charge resistance and discharge resistance with depth-of-discharge.

$$P_{\text{discharge}} = \frac{V_{\min}(\text{OCV}_{\text{discharge}} - V_{\min})}{R_{\text{discharge}}} \quad (3)$$

where $\Delta I_{\text{discharge}} = I_{\text{d1}} - I_{\text{d2}}$ and $\Delta V_{\text{discharge}} = V_{\text{d1}} - V_{\text{d2}}$. V_{d1} and V_{d2} are the corresponding voltages at I_{d1} and I_{d2}. $\text{OCV}_{\text{discharge}}$ is the open-circuit voltage before the discharge current I_{d1}. Similarly, the charge resistance and the maximum power were calculated using the following equations with the maximum voltage ($V_{\max}$) of 16 V.

$$R_{\text{charge}} = \frac{\Delta V_{\text{charge}}}{\Delta I_{\text{charge}}} \quad (4)$$

$$P_{\text{charge}} = \frac{V_{\max}(V_{\max} - \text{OCV}_{\text{charge}})}{R_{\text{charge}}} \quad (5)$$

where $\Delta I_{\text{charge}} = I_{\text{c2}} - I_{\text{c1}}$ and $\Delta V_{\text{charge}} = V_{\text{c2}} - V_{\text{c1}}$. $\text{OCV}_{\text{charge}}$ are the open-circuit voltage before the charge current I_{c1}. Note that there is an assumption for the discharge resistance and charge resistance used to determine the maximum discharge power (Eq. (3)) and maximum charge power (Eq. (5)). At a given DoD, the discharge resistance ($R_{\text{discharge}} = \Delta V_{\text{discharge}}/\Delta I_{\text{discharge}}$) and charge resistance ($R_{\text{charge}} = \Delta V_{\text{charge}}/\Delta I_{\text{charge}}$) are considered constant irrespective of the amplitude of the current pulse (i.e., ΔI), provided that the battery temperature is unchanged. Therefore, the maximum discharge current and the maximum charge current, by which the battery voltage reaches $V_{\min}$ and $V_{\max}$ at 10 s, can be calculated by $(\text{OCV}_{\text{discharge}} - V_{\min})/R_{\text{discharge}}$ and $(V_{\max} - \text{OCV}_{\text{charge}})/R_{\text{charge}}$, respectively. Consequently, the maximum discharge power can be determined from the minimum voltage and maximum discharge current (i.e., $V_{\min} \times (\text{OCV}_{\text{discharge}} - V_{\min})/R_{\text{discharge}}$), while the maximum charge power from the maximum voltage and maximum charge current (i.e., $V_{\max} \times (V_{\max} - \text{OCV}_{\text{charge}})/R_{\text{charge}}$).

The changes in open-circuit voltage, charge and discharge resistances with depth-of-discharge are shown in Fig. 10. The open-circuit voltage decreases linearly with the increased depth-of-discharge and therefore, one usually uses the value of open-circuit voltage during cycling to predict the SoC of the battery. The charge resistance of the battery also decreases with increasing depth-of-discharge, but only up to 40% DoD. The resistance then remains virtually unchanged between 40 and 80% DoD and starts to increase at DoD greater than 80%. This is understandable because the charge resistance determined by a 10-s constant current pulse will compose of two components. One is ohmic resistance and other is charge-reaction resistance (or Faradaic-reaction resistance). The ohmic resistance increases, while the charge-reaction resistance decreases with the increase of depth-of-discharge as shown schematically in Fig. 11. Thus, the decrease in charge resistance (i.e., combined ohmic and charge-reaction resistances) up to 40% DoD is due to the decrease in charge-reaction resistance. On the other hand, the increase in charge resistance at DoD greater than 80% is due to the increase in ohmic resistance. Similarly, the discharge resistance also composes of two components, namely ohmic resistance and discharge-reaction resistance. Neverthe-

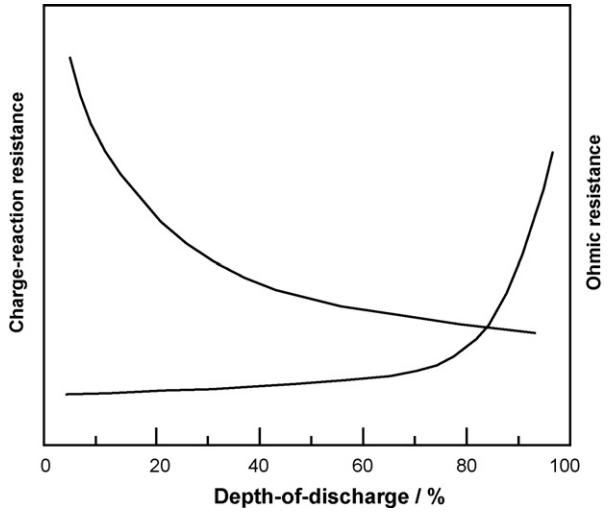

Fig. 11. Changes in charge-reaction and ohmic resistances with depth-of-discharge of the battery.

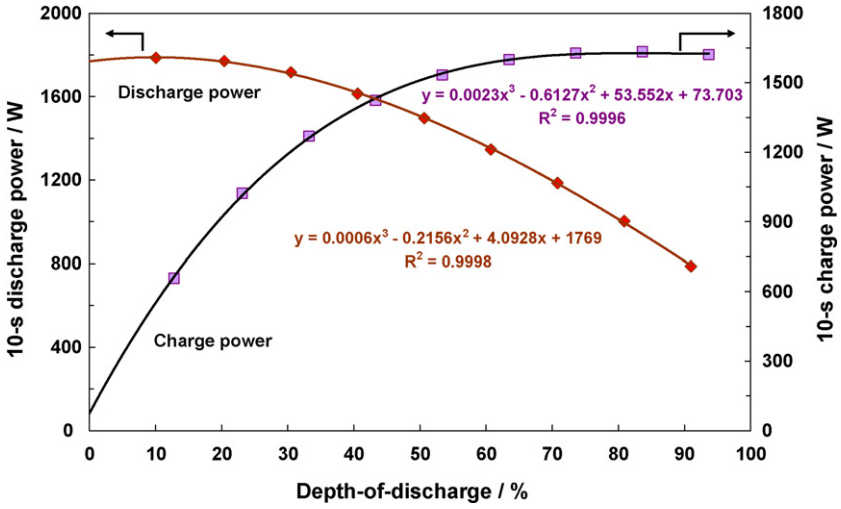

Fig. 12. Changes in discharge and charge power with depth-of-discharge.

less, both the ohmic and the reaction resistances increase with the increase of depth-of-discharge and therefore, the overall discharge resistance also increases.

The changes in discharge and charge power with depth-of-discharge of the battery are shown in Fig. 12. It can be seen that the discharge power decreases while the charge power increases with increasing depth-of-discharge. In the US FreedomCAR Battery Test Manual, there are two power-assist systems, namely, minimum and maximum power-assist. The targets, such as power, available energy, etc., set for these two systems are based upon the full-size vehicle battery pack. Therefore, in order to compare the data obtained from the single battery in this study with the targets set for the full-size vehicle battery, the discharge and charge power of the single battery should be scaled by a factor, called the battery-size factor (BSF). The battery size factors were determined based upon the procedures described in the US FreedomCAR Battery Test Manual [15] and the values are 21 for the minimum power-assist system and 35 for the maximum power-assist system, respectively.

The discharge and charge power are scaled by the battery-size factor of 21 for minimum power-assist system and plotted against the depth-of-discharge (Fig. 13). According to the US FreedomCAR, the discharge and charge power required by the minimum power-assist system are 25 and 20 kW, respectively. Therefore, a straight line is drawn between 25 and 20 kW and this line meets the charge–power and discharge–power curves at 21 and 70.5% DoD. This indicates that to meet the discharge power of 25 kW and charge power of 20 kW, the Ultrabattery pack should operate within the 21–70% DoD window. Clearly, with the integration of supercapacitor electrode, the operational range of the Ultrabattery is now between 21 and 70% DoD, instead of between 30 and 70% DoD for the VRLA battery mentioned in Section 1.

Similarly, the power-versus-energy removed at 1-h rate, which are scaled by the BSF, is shown in Fig. 14. The available energy is the energy difference at the two intersection points between the charge– and discharge–power curves and the straight line drawn between 25 and 20 kW. The value is found to be 940 Wh, which is over three times greater than the energy goal of 300 Wh set for the minimum power-assist system.

For the maximum power-assist system, the power-versus-energy removed at 1-h rate scaled by a BSF of 35 is shown in

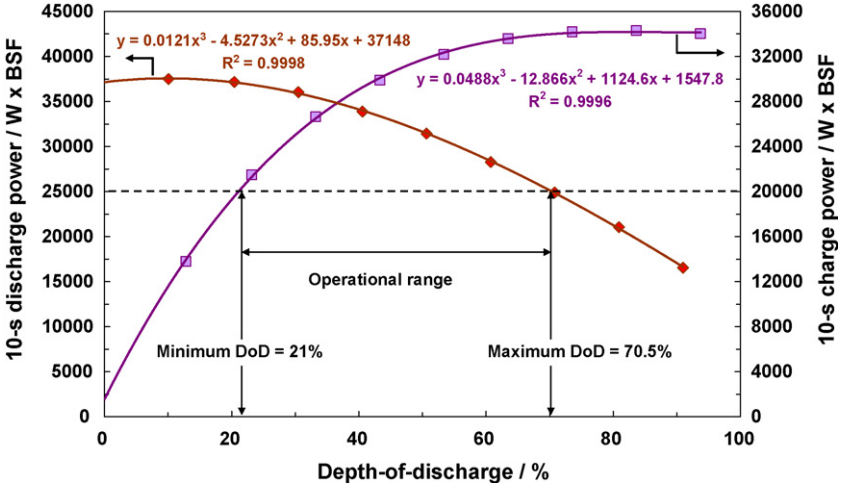

Fig. 13. Changes in discharge and charge power (scaled by battery-size factor of 21) with depth-of-discharge.

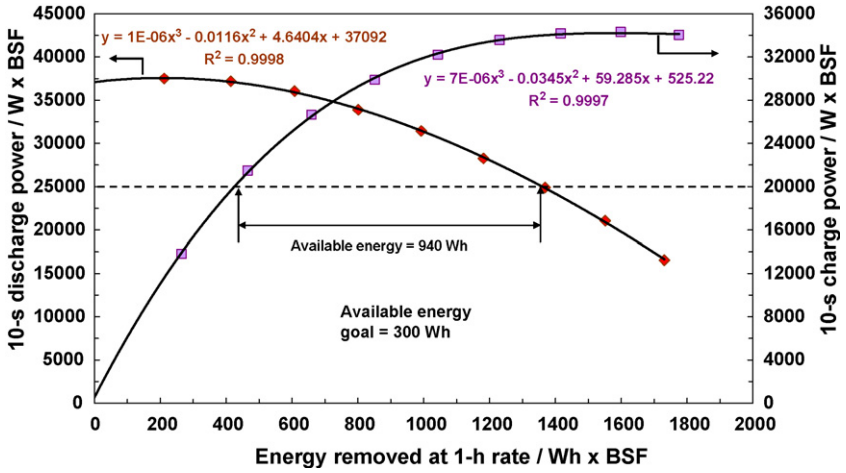

Fig. 14. Changes in discharge and charge power with energy removed at 1-h rate (scaled by BSF of 21).

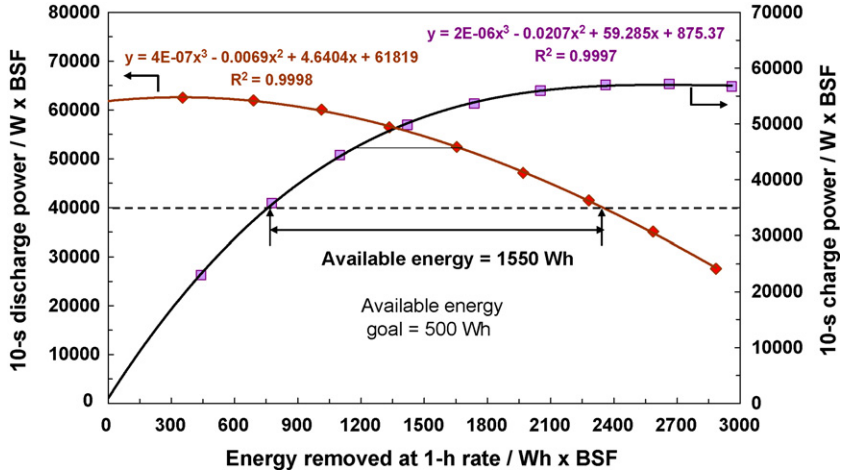

Fig. 15. Changes in discharge and charge power with energy removed at 1-h rate (scaled by BSF of 35).

Fig. 15. The requirements of the discharge and charge power for this system are 40 and 35 kW, respectively. The available energy is the energy difference at the two intersection points between the charge– and discharge–power curves and the straight line drawn between 40 and 35 kW. The value is found to 1550 Wh. Similar to the minimum power-assist system, the available energy is again three times greater than the goal of 500 Wh set for the maximum power-assist system.

5.3. Cold cranking

The profile used to evaluate the cold-cranking performance of the battery pack is shown in Fig. 16. The profile consists of three consecutive 2-s power pulses. There is a 10-s rest between each pulse. The amplitudes of the pulse are 5 kW for minimum power-assist and 7 kW for maximum power-assist, respectively. The test procedure is as follows.

(i) At ambient temperature, discharge the battery at 1-h rate to the maximum DoD where the available energy goal is met. These are 49% for minimum power-assist and 51% for maximum power-assist, respectively.
(ii) Reduce the battery temperature to −30 °C.
(iii) Perform the cold-cranking profile with power values equal to 5 kW divided by the BSF of 21 for the minimum power-assist and 7 kW divided by the BSF of 35 for the maximum power-assist.
(iv) Record the voltage and current before and at the end of each power pulse.

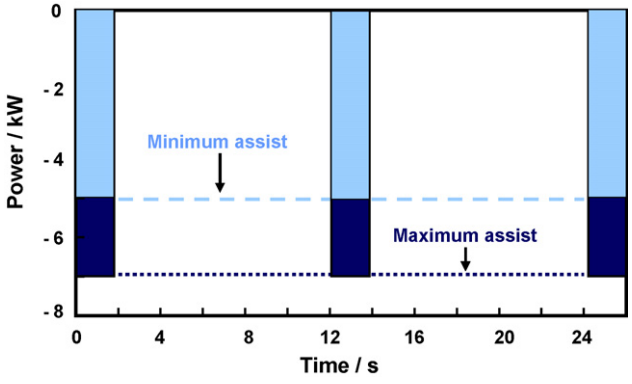

Fig. 16. Profile used to evaluate the cold cranking performance of Ultrabattery.

Table 3
Cold-cranking performance of Ultrabattery

	Minimum power-assist (kW)	Maximum power-assist (kW)
Goals	5	7
Measured values	5.4 (1), 5.2 (2), 5.1 (3)	10.5 (1), 11.3 (2), 11.3 (3)

(v) Calculate each of the three cold-cranking power pulses using Eq. (3) in Section 5.2 with the minimum voltage of 9 V and multiply the results by the BSF of 21 or 35.

The goal and the measured values for minimum and maximum power-assist are given in Table 3. It can be seen that all the measured values meet or exceed the targets set for either minimum or maximum power-assist systems. It needs to be stated here that the minimum voltage, we used for this test is a conservative 9 V, instead of 7.2 V normally used to evaluate the cold-cranking performance of the lead-acid battery.

5.4. Self-discharge

The self-discharge performance of the Ultrabattery was evaluated at 30 °C. The test procedure is as follows.

(i) After full charge, determine the 1-h capacity of the battery, followed by a recharge, record $Wh_{c/1\ before\ test}$.
(ii) Discharge the battery down to 30% DoD, record $Wh_{30\%\ DoD}$ and allow it to stand in an open-circuit condition for 7 days; during the standing time, the battery must be disconnected from the test equipment.
(iii) Discharge the battery for its remaining (residual) capacity at 1-h rate, record $Wh_{residual}$.
(iv) Calculate the self-discharge by using the following equation.

$$SD = \left[\frac{(Wh_{c/1\ before\ test} - (Wh_{30\%\ DoD} + Wh_{residual}))}{7\ days}\right] \times BSF \quad (6)$$

The goals and measured values are given in Table 4. It can be seen that after 7-day standing, the Ultrabattery shows an energy gain, not energy loss even though the above test procedure has been repeated three times.

Table 4
Self-discharge performance of prototype Ultrabattery

	Minimum power-assist ($Wh\ day^{-1}$)	Maximum power-assist ($Wh\ day^{-1}$)
Goal (at 30 °C)	−50	−50
Measurement (at 30 °C)	+3.90 (1st), +6.38 (2nd), +4.28 (3rd)	+6.51 (1st), +10.64 (2nd), +7.14 (3rd)
Measurement (at 40 °C)	−7.42	−12.37

Note: minus value indicates energy loss, while plus value indicates energy gain.

Therefore, the test was conducted again, but with slight modifications. After full charge, the 1-h capacity of the battery was determined, followed by a recharge. The battery was then allowed to stand in an open-circuit condition for 23 days, instead of 7 days. Furthermore, the test was performed at 40 °C, instead of 30 °C. After 23 days, the battery was discharged for its remaining residual capacity. Results show that with this procedure, the Ultrabattery shows an energy loss of −7.42 Wh per day for the minimum power-assist system and $-12.37\ Wh\ day^{-1}$ for the maximum power-assist system (see Table 4). These values are well below the self-discharge goal set (i.e., $50\ Wh\ day^{-1}$) for both power-assist systems. In addition, the results also show that allowing the Ultrabattery to stand at open-circuit and partial-state-of-charge conditions for 7 days may not be long enough to cause any apparent self-discharge of the battery.

From the above results, it is clear that the Ultrabattery technology has met or exceeded the targets of power, available energy, cold cranking and self-discharge required by the minimum and maximum power-assist systems.

6. Cycling performance of prototype Ultrabatteries

The cycling performance of Ultrabattery was evaluated using: (i) simplified discharge and charge profile to simulate the micro-HEV driving conditions; (ii) 42-V profile to simulate the mild-HEV driving conditions [16,17]; (iii) EUCAR power-assist and RHOLAB profiles to simulate the medium-HEV driving conditions [18–20]. Furthermore, in the interests of expediency, the battery was subjected to each of the above profiles repetitively until the voltage reached the specified cut-off value. Thus, it is not a real cycle-life test, but rather a screening test.

6.1. Simplified discharge and charge profile

The simplified discharge and charge profile used to simulate the micro-hybrid driving conditions is shown in Fig. 17. The profile composes of a discharge at 3*C* A for 60 s and a charge at a constant voltage of 2.5 V per cell with maximum current of 3*C* A for 62 s. There are two rest times of 10 s each in between

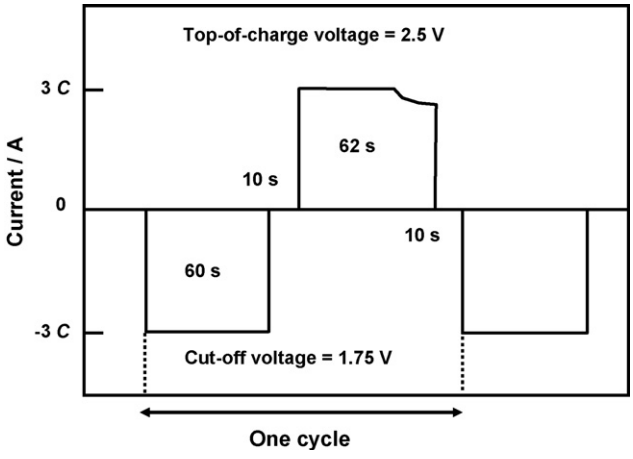

Fig. 17. Simplified discharge and charge profile with top-of-charge voltage of 2.5 V per cell and cut-off voltage of 1.75 V per cell.

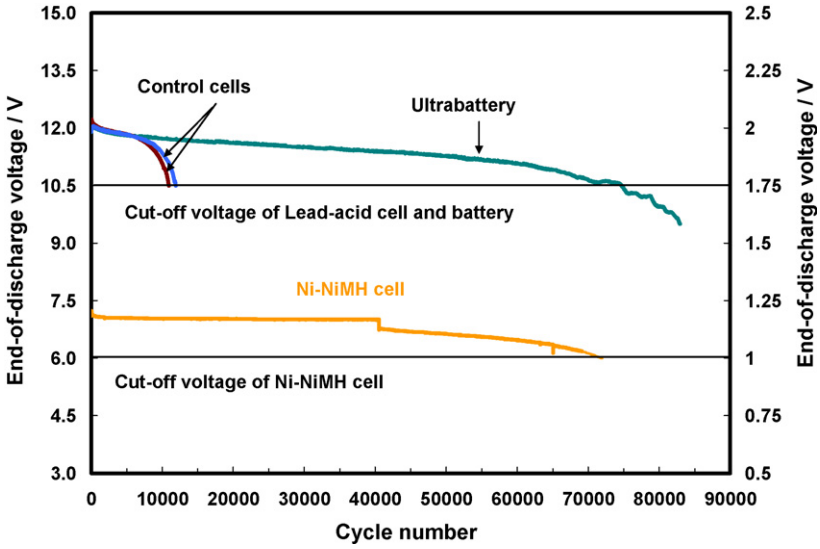

Fig. 18. Changes in end-of-discharge voltages of control cells, Ultrabattery and Ni–MH cell with cycling.

discharge and charge or charge and discharge pulses. The full-charge cell or battery was subjected to this profile repetitively at 40 °C until the voltage of the cell reached 1.75 V per cell.

The performance of the control cells and the Ultrabattery are shown in Fig. 18. The end-of-discharge (EoD) voltages of control cells and Ultrabattery all decrease with cycling, but the rate of decrease is slower for the latter battery. Accordingly, two control cells reach the cut-off voltage at about 12,000 and 13,000 cycles, respectively. On the other hand, the Ultrabattery reaches the cut-off value at about 75,000 cycles. It needs to be stated here that all the control cells used in this study are the present state-of-the art cells in which the negative plates were doped with carbon at level of about 2 wt.%.

For comparison, a Ni–MH cell, which is presently used in the Honda Insight HEV, was also subjected to this test (Fig. 18). Up to 40 000 cycles, the Ni–MH cell was cycled with discharge and charge current of 2*C*, instead of 3*C* by mistake. Therefore, the discharge and charge current was changed to 3*C* after 40,000 cycles. In the same way as the Ultrabattery, the EoDV of the Ni–MH cell also decreases slowly with cycling and reaches its corresponding cut-off value of 1 V at about 73,000 cycles.

Another simplified discharge and charge profile was also used to evaluate the performance of the Ultrabattery (Fig. 19). The differences between this profile and the profile shown in Fig. 17 are the current amplitude, top-of charge voltage and cut-off voltage. The discharge and charge current in this profile are reduced to 2*C*, while the top-of-charge voltage is increased to 2.83 V per cell. Furthermore, the cut-off voltage is high, namely, 1.83 V per cell, instead of 1.75 V used in the previous profile. Initially, the cell or battery was discharged to 50% SoC and then subjected to this profile repetitively until the voltage reached 1.83 V per cell. The test would also be terminated when the voltage reached 2.83 V per cell during the charging part of the profile.

The changes in end-of-discharge and charge voltages of the control cell and the Ultrabattery are shown in Fig. 20. Both the end-of-discharge and charge voltages of the control cell decrease with cycling and the discharge voltage reaches the lower voltage limit at 4300 cycles. Similarly, both the end-of-discharge and charge voltage of the Ultrabattery also decrease with cycling. Nevertheless, the rate of decrease in the end-of-discharge and charge voltage of the Ultrabattery is much slower than that of the control cell. Consequently, the Ultrabattery completed about 18,000 cycles.

From the above results, it can be seen that the cycling performance of the Ultrabattery is at least four times longer than that of the control cells and is comparable with that of the Ni–MH cell.

6.2. 42-V profile

The 42-V profile used to simulate the mild-hybrid driving conditions is shown in Fig. 21 [16,17]. The duration of the profile is about 2.35 min. The profile is composed of several current steps that simulate the power requirements of the battery during vehicle operation, namely, idle–stop, cranking, power-assist,

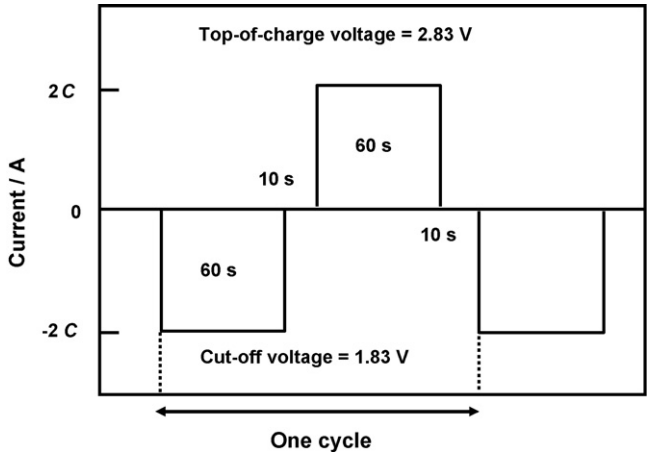

Fig. 19. Simplified discharge and charge profile with top-of-charge voltage of 2.5 V per cell and cut-off voltage of 1.75 V per cell.

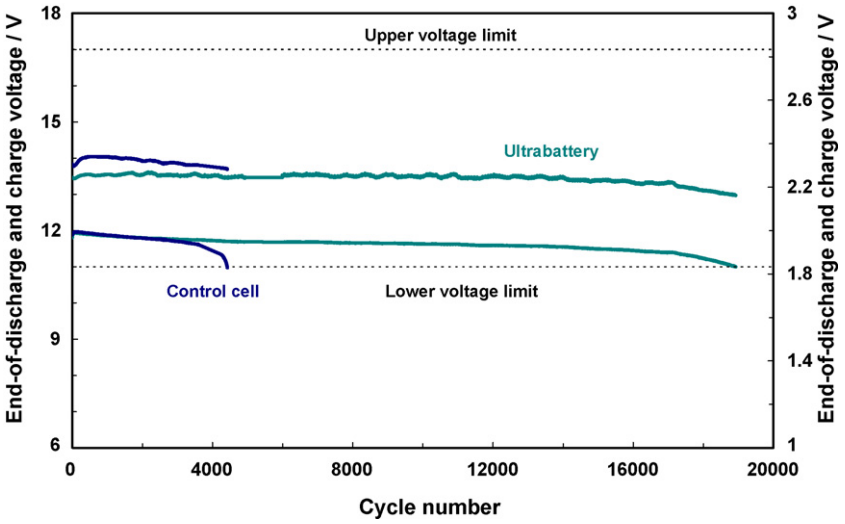

Fig. 20. Changes in end-of-discharge and charge voltages of control cell and Ultrabattery.

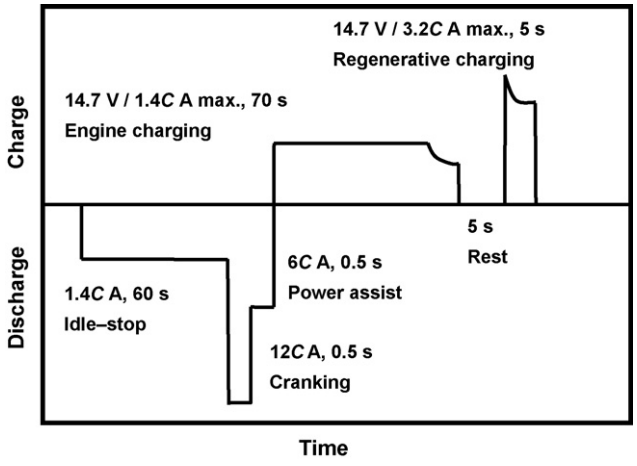

Fig. 21. The 42-V profile used to simulate the driving conditions of mild-HEV.

engine charging, and regenerative charging. The critical steps are the cranking and regenerative braking periods and over which the battery must deliver a current of 12*C* and receive a maximum current of 3.2*C*. During the cranking period, the voltage of the battery will fall to its lowest level.

The full-charge cell or battery was subjected to this profile repetitively at 40 °C until the minimum voltage reached 1.33 V per cell.

The cycling performance of the control cell and the Ultrabattery is shown in Fig. 22. The minimum voltage of the control cell reaches the cut-off value of 1.33 V per cell after 13,000 cycles, while that of the Ultrabattery is still well above the cut-off value. The Ultrabattery has cycled up to 109,000 cycles and is still in healthy condition. Again, the cycling performance of the Ultrabattery is significantly longer than that of the control cell. Furthermore, this performance also shows much longer than the VRLA battery superimposed with high-frequency pulses, which was developed previously in the CSIRO laboratories (e.g., 42,000 cycles [5]).

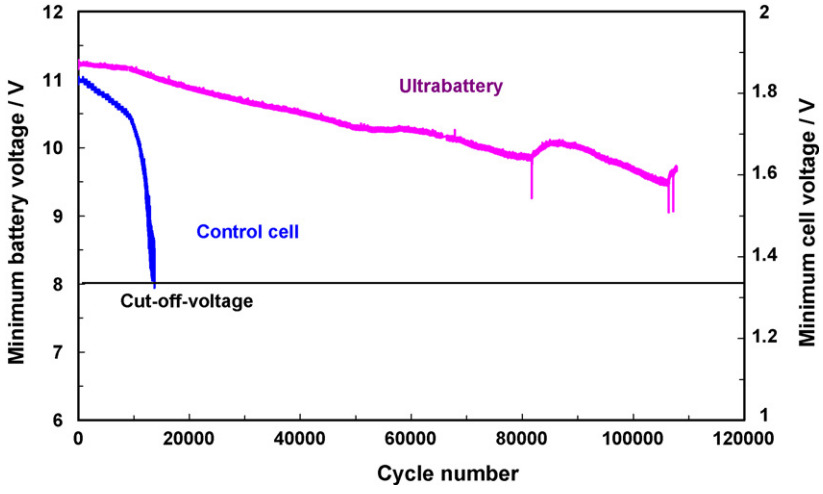

Fig. 22. Cycling performance of control cell and Ultrabattery under 42-V profile.

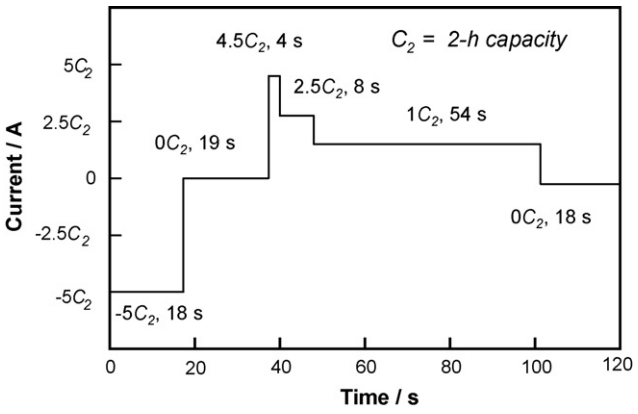

Fig. 23. EUCAR power-assist profile.

6.3. EUCAR profile

The EUCAR power-assist profile used to simulate the driving conditions of the medium-hybrid vehicle is shown in Fig. 23 [18]. The profile comprises a discharge to simulate the power-assist (i.e., $5C_2$ A, C_2 = 2-h capacity), a rest period and a recharge with three stepped currents (i.e., $4.5C_2$ A, $2.5C_2$ A and C_2 A, repetitively) to simulate the charging from regenerative braking and the engine.

The cell or battery was discharged initially at C_2 rate to 60% state-of-charge and then was subjected to this profile repetitively at 40 °C until the voltage reached 1.77 V per cell. During cycling, all the cells and batteries were maintained at 40 °C and the top-of-charge voltage was regulated at 2.45 V per cell.

The cycling performance of a control cell and an Ultrabattery is shown in Fig. 24. The voltage of the control cell decreases gradually with cycling and reaches the cut-off value of 1.77 V per cell after 32,500 cycles. On the other hand, the voltage of the Ultrabattery remains very stable with cycling and the battery has cycled up to 132,000 cycles and is still in a healthy condition.

A Ni–MH cell was also subjected to this test. Similar to the Ultrabattery, the Ni–MH cell has cycled up to 132,000 cycles and is still in a healthy condition. Nevertheless, a cut-off voltage of 0.95 V was used for Ni–MH cell under this profile, instead of

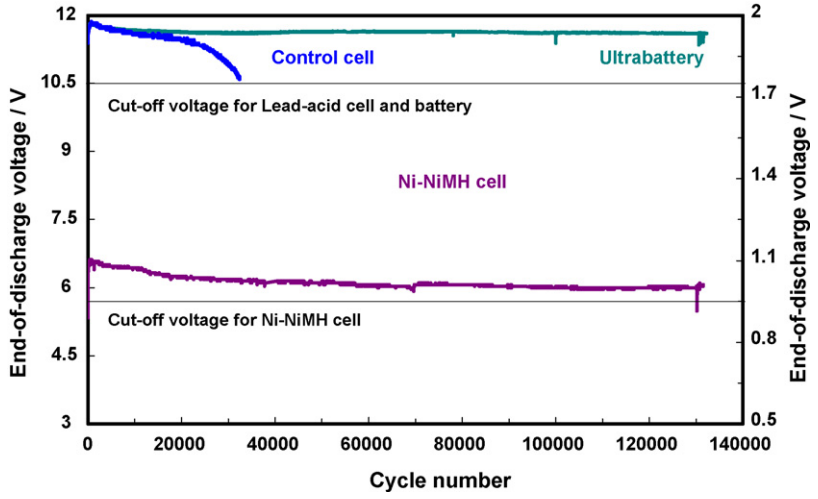

Fig. 24. Cycling performance of control cell, Ultrabattery and Ni–MH cell under EUCAR profile.

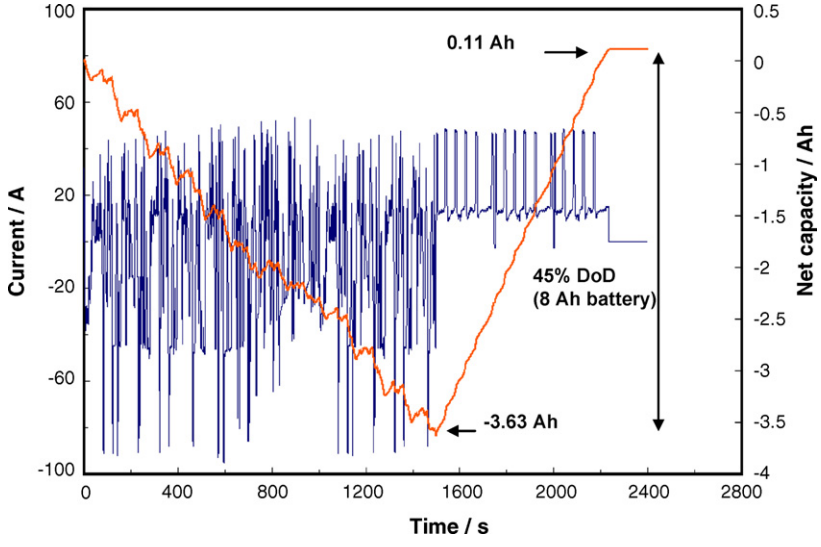

Fig. 25. RHOLAB profile.

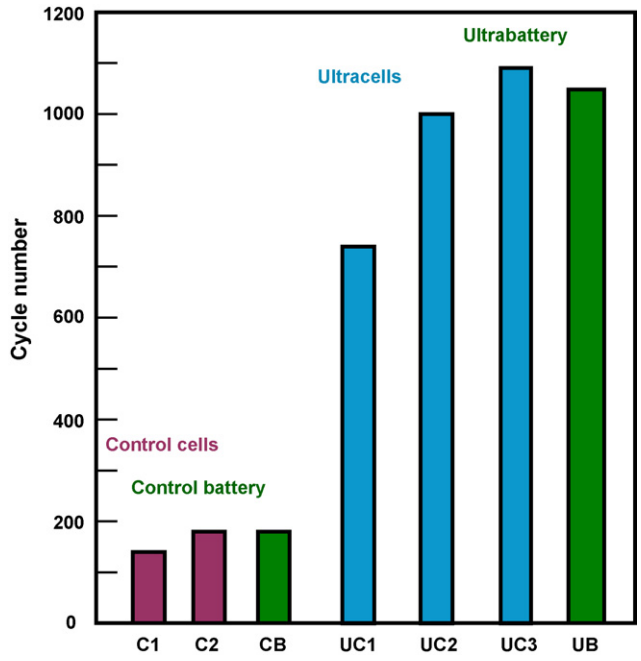

Fig. 26. Cycling performance of cells and batteries under RHOLAB profile.

1 V used for the simplified discharge and charge profile (Section 6.1).

6.4. RHOLAB profile

The profile used to simulate the combined high-speed and hill-climbing driving conditions is shown in Fig. 25. This profile was developed by the RHOLAB project [19,20]. The duration of a profile, or a cycle, is about 2400 s. There are three levels of current during the discharge part of the profile. The highest current is for acceleration, while the medium and the lowest currents are for high speed and cruise driving. There are also two levels of current during the charging part of the profile. The low current is from engine charging, while the high charging current is from the regenerative braking. At each cycle, the 8-Ah cell (5-h capacity) is required to discharge down to 45% DoD. Accordingly, this profile is much more severe than the other profiles used in this study. Initially, the cell or battery was discharged to 80% SoC and then subjected to the profile repetitively until the minimum cell voltage reached 0 V.

The cycling performance of cells and batteries under the RHOLAB profile is shown in Fig. 26. It can be seen that the control cells and battery achieved 150–180 cycles, while the Ultracells and Ultrabattery achieved 750–1100 cycles. This demonstrates clearly that the cycling performance of Ultracells and Ultrabattery is at least four times longer than that of the control cells and battery.

7. Conclusions

This study has highlighted the importance of protecting the negative plates of the VRLA battery from discharge and charge at the high rates under HEV duty. The unique CSIRO's approach is to combine an asymmetric supercapacitor and a lead-acid battery in one unit cell without the need for extra electronic controls—Ultrabattery. Prototype Ultrabatteries have been produced and evaluated under a variety of laboratory tests. Results show that the initial and cycling performance of the prototype Ultrabatteries has the following features and benefits.

(i) The Ultrabatteries can operate at a wider partial-state-of-charge window than that of the VRLA batteries under HEV applications and have met or exceeded the targets of power, available energy, cold cranking and self-discharge specified for both minimum and maximum power-assist systems.
(ii) The Ultrabatteries show at least four times longer in cycling performance than the control VRLA lead-acid cells and batteries. Furthermore, this promising performance may be comparable with that of Ni–MH cells, but with greatly reduced cost.

Acknowledgement

This work has been supported by the Advanced Lead-Acid Battery Consortium, Research Triangle Park, NC, USA.

References

[1] L.T. Lam, C.G. Phyland, D.A.J. Rand, A.J. Urban, ALABC Project C2.0, Novel Technique to Ensure Battery Reliability in 42-V PowerNets for New-generation Automobiles, Progress Report: August 2001–January 2002, CSIRO Energy Technology, Investigation Report ET/IR480R, March 2002, 19 pp.
[2] L.T. Lam, N.P. Haigh, C.G. Phyland, D.A.J. Rand, A.J. Urban, ALABC Project C 2.0, Novel Technique to Ensure Battery Reliability in 42-V PowerNets for New-generation Automobiles, Final Report: August 2001–November 2002, CSIRO Energy Technology, Investigation Report ET/IR561R, December 2002, 39 pp.
[3] L.T. Lam, N.P. Haigh, C.G. Phyland, T.D. Huynh, D.A.J. Rand, ALABC Project C 2.0, Novel Technique to Ensure Battery Reliability in 42-V PowerNets for New-generation Automobiles, Extended Report: January–April 2003, CSIRO Energy Technology, Investigation Report ET/IR604R, May 2003, 23 pp.
[4] A.F. Hollenkamp, W.G.A. Baldsing, S. Lau, O.V. Lim, R.H. Newnham, D.A.J. Rand, J.M. Rosalie, D.G. Vella, L.H. Vu, ALABC Project N1.2, Overcoming Negative-plate Capacity Loss in VRLA Batteries Cycled under Partial State-of-Charge Duty, Final Report: July 2000–June 2002, CSIRO Energy Technology, Investigation Report ET/IR491R, June 2002, 47 pp.
[5] L.T. Lam, N.P. Haigh, C.G. Phyland, T.D. Huynh, J. Power Sources 144 (2005) 552–559.
[6] L.T. Lam, N.P. Haigh, C.G. Phyland, A.J. Urban, J. Power Sources 133 (2004) 126–134.
[7] K. Nakamura, M. Shiomi, T. Takahashi, M. Tsubota, J. Power Sources 59 (1996) 153–157.
[8] M. Shiomi, T. Funato, K. Nakamura, T. Takahashi, M. Tsubota, J. Power Sources 64 (1997) 147–152.
[9] K. Honbo, E. Hoshi, A. Miura, T. Hiraswa, In-situ Analyses of Negative Electrodes for Lead-Acid Batteries on Charge–Discharge Reaction by Atomic Force Microscopy, Shin-Kobe Technical Report No. 12, February 2002, pp. 3–10.
[10] R.H. Newnham, W.G.A. Baldsing, A.F. Hollenkamp, O.V. Lim, C.G. Phyland, D.A.J. Rand, J.M. Rosalie, D.G. Vella, Advancement of Valve-Regulated Lead-Acid Battery Technology for Hybrid-Electric and Electric Vehicles, ALABC Project C/N 1.1, Final Report: July 2000–June 2002,

CSIRO Energy Technology, Investigation Report ET/IR520R, August 2002, 44 pp.
[11] L.T. Lam, N.P. Haigh, O.V. Lim, T. Lwin, C.G. Phyland, D.G. Vella, ALABC Project TE-1, Influence of Trace Elements, Plate-Processing Conditions, and Electrolyte Concentration on the Performance of Valve-Regulated Lead-Acid Batteries at High Temperatures and Under High-Rate Partial-State-of-Charge Operation, Final Report: August 2003–July 2005, CSIRO Energy Technology, Investigation Report ET/IR809R, July 2005, 43 pp.
[12] Australian Patent Application No. 2003905086.
[13] International Patent Application No. PCT/AU2004/001262.
[14] L.T. Lam, R. Louey, J. Power Sources 158 (2006) 1140–1148.
[15] US FreedomCAR Battery Test Manual, DOE/ID-11069, October 2003.
[16] T. Noda, K. Hata, K. Yamanaka, M. Tsubota, Paper Presented at the Ninth Asian Battery Conference, Bali, Indonesia, September, 2001.
[17] L.T. Lam, R. Louey, N.P. Haigh, O.V. Lim, D.G. Vella, C.G. Phyland, L.H. Vu, ALABC Project DP 1.1, Production and Test of Hybrid VRLA Ultrabattery Designed Specifically for High-Rate Partial-State-of-Charge Operation, Progress Report: August 2006–October 2006, CSIRO Energy Technology, Investigation Report ET/IR911R, October 2006, 38 pp.
[18] F. Trinidad, C. Gimeno, J. Gutierrez, R. Ruiz, J. Sainz, J. Valenciano, J. Power Sources 116 (2003) 128–140.
[19] A. Cooper, J. Power Sources 133 (2004) 116–125.
[20] A. Cooper, J. Power Sources 144 (2005) 385–394.